Meccanica (2023) 58:2165–2176
https://doi.org/10.1007/s11012-023-01719-5

Investigating frictional contact behavior for soft material robot simulations

Rebecca Berthold · Jessica Burgner-Kahrs · Matthias Wangenheim · Stephanie Kahms

Received: 19 June 2023 / Accepted: 9 October 2023 / Published online: 7 November 2023

Abstract The ability to interact safely with the environment is known as one of the major advantages of soft robots (SRs). Due to their low material stiffness, these continuously deformable robots offer inherent flexibility. These advantages make them suitable for application that involve human-robot collaboration in industrial settings as well as medical application such as minimally invasive surgery. To date only few research groups have analyzed the contact and frictional behavior of soft robots. In fact, the contact behavior is often oversimplified or neglected. Motivated by the idea to bridge this gap, this work presents measurements and the resulting coefficient of friction (COF) for silicone rubbers that are widely used in the field of SRs and different contact partners which depend on contact pressure and ambient temperature. From these measurements, a more representative contact model is established and used to more accurately simulate soft material robots' frictional contact behavior. Moreover the influence of friction and therefore the need to implement frictional behavior is demonstrated for a typical application of a SR.

Keywords Soft robotics · Elastomers · Friction · Contact modeling · Friction measurement

Abbreviations

SR	Soft robot
COF	Coefficient of friction
FEA	Finite element analysis
SPA	Soft pneumatic actuator

1 Introduction

Inspired by nature, soft robots (SRs) are an aspiring field of research. Compared to their rigid counterparts, SRs are defined by their low material and structural stiffness which makes them suitable to interact safely in complex or unknown environments. Particularly, SRs are inherently safe to use in human-robot interaction due to their softness and the associated integrated compliance. The idea behind this bioinspired technology is to mimic specific functionalities such as the flexibility of an octopus or the movement of a worm [1]. These

R. Berthold (✉) · M. Wangenheim · S. Kahms
Institute of Dynamics and Vibration Research, Leibniz University Hannover, An der Universität 1, Garbsen 30823, Niedersachsen, Germany
e-mail: berthold@ids.uni-hannover.de

M. Wangenheim
e-mail: wangenheim@ids.uni-hannover.de

S. Kahms
e-mail: kahms@ids.uni-hannover.de

J. Burgner-Kahrs
Continuum Robotics Laboratory, Department of Mathematical and Computational Sciences, University of Toronto, 3359 Mississauga Road, Mississauga L5L 1C6, Ontario, Canada
e-mail: jessica.burgnerkahrs@utoronto.ca

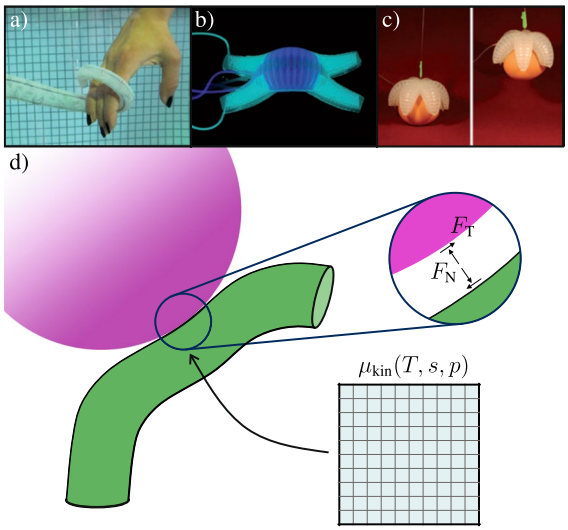

Fig. 1 The figure gives an overview of typical bioinspired SRs (**a**) [10] whose functionalities rely on frictional behavior such as crawling (**b**) [11] or gripping (**c**) [12]. During contact, the COF can vary depending on e.g. temperature, sliding distance or contact pressure. The schematic SR (**d**) showcases a contact scenario where a friction map, that captures these dependencies is used

advantages make SRs well suited to use in medical applications [2] or in highly constrained environments as for example shown in [3]. Soft materials have enabled the development of numerous types of actuators, for example, fluid-driven actuators [4]. In the past years, the field of SRs developed rapidly, presenting new approaches of manufacturing, modeling, and controlling these robots. Yet the field has not been able to significantly contribute to industrial applications according to [5]. One approach to enable new and meaningful developments which will allow the SRs field to go beyond fundamental research is to establish toolboxes and open source resources which future research can build upon [6–8]. As the main motivation behind SRs is strongly tied to their favourable environmental contact behavior, understanding the phenomena related to contact and in particular friction is essential. [9] mention contact modeling as a challenge that has to be addressed in future research in the field of soft material robotics. In Fig. 1 three SRs that represent typical fields in soft robotics are shown. While there exist various designs of SRs, they all experience similar contact and frictional behavior when interacting with their respective environments.

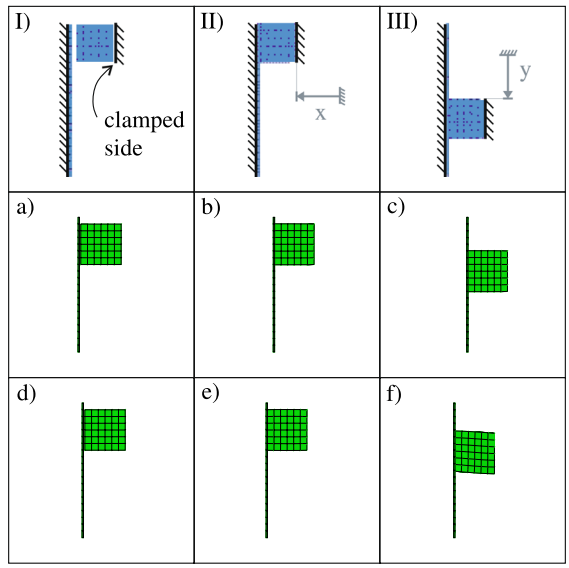

Fig. 2 Simulation steps for contact simulation of a toy example (I–III). In the first step (A), the soft cube is placed at a distance from a wall. In the second step (B), the cube is brought into contact with the wall by applying a displacement boundary condition as indicated by the arrow in the x direction. In the last step (C), relative motion between the cube and the wall is implemented. The results show the soft cube sliding on a rigid wall with non-frictional contact **a**–**c** and frictional contact **d**–**f**

1.1 On the importance of modeling friction

While the soft robotics community acknowledges the importance of friction in modeling SRs [9, 13], the frictional behavior of commonly used materials, e.g. [8, 14–17], has not been investigated in a systematic way.

In order to clearly demonstrate the influence of modeling friction, the contact behavior is investigated using a toy example. For this purpose, a cube with an edge length of 30 mm and placed at a distance of 1 mm from a rigid plate is modeled in the commercially available software *ABAQUS*, as shown in Fig. 2 (I–III). The material for the cube is a soft silicon rubber (Sect. 4.1.1) that represents the low material stiffness which is typical for SRs. The cube's clamped side is then moved by x=1.7 mm so that it comes into contact with the plate. Afterwards the cube is moved along the plate's longitudinal axis by y=2 cm in a static simulation. For the contact setup, the penalty contact is used for both the normal and tangential contact behavior. Here the COF based on the

Coulomb friction model can be defined as described in [18]. For this example a COF of 0.5 is chosen to represent the frictional behavior.

In Fig. 2a–f, the results of this simulation are shown for non-frictional contact (a–c) and frictional contact (d–f). The results demonstrate, that the deformation of the cube strongly depends on the frictional behavior. While no tangential forces are transmitted without friction, the tangential forces for the frictional contact lead to a significant deformation of the cube. For frictional contact, the displacement differs from that of the non-frictional case by about 2 mm for a 20 mm displacement, which corresponds to a 10% difference. Also, the total area in contact varies by nearly 20% between the non-frictional and frictional simulations according to the history output variable *CNAREA*. With regard to applications such as gripping, this result underlines the need to include friction, as this not only enables the gripping mechanism itself, but also significantly affects the contact surface.

These simulations demonstrates the effect of friction on a toy example to highlight the importance of implementing frictional behavior for tasks such as gripping. In the field of SRs, contact modeling is only implemented in some models so far. Some research groups use non-frictional contact for a simple approximation [19, 20]. According to [21], non-frictional contact can be assumed for medical applications as insufficient data is available and the COF is sufficiently small to be neglected. While this assumption holds for very low COFs, the authors acknowledge that suitable data is not available so far. More recently [22] presented a dynamic model based on discrete differential geometry that accounts for surface roughness as well as frictional contact for SRs. In this paper, the authors measure and implement a single COF. In [13], an overview is given among other things on the modeling and characterization of materials including friction. The overview shows that friction is only investigated and used in few works so far. For different SRs, the assumption of non-frictional contact is no longer possible as their operating principle rely on frictional behavior as demonstrated with the toy example. For example the locomotion of snakelike robots or crawlers as well as various grippers rely on friction [23–26].

In [27], a framework for dynamic modeling of robots that mimic the function of biological cilia is discussed. The framework is based on a Kirchhoff rod model where the frictional force is incrementally applied if contact occurs to ensure smooth increase. At the same time, depending on the robot and application, friction needs to be minimized in some cases in order to minimize energy loss while obtaining the locomotion [26, 28]. These conflicting goals demonstrate that each robot's frictional characteristics can be optimized to fulfill a designated task.

Therefore, there is a need for simulations which employ contact models that use reasonable experimentally-informed frictional behavior. Especially when aiming for application that rely on frictional behavior, a good estimation of the coefficient of friction (COF) is required to, e.g., forecast the normal force needed to pick up an object or the actuation needed to realize a specified locomotion. On a broader scale, in [29] contact modeling for flexible systems that undergo large deformation is presented. In contrast to approaches that introduce artificial factors to ensure a smooth increase of contact forces such as the penalty method, this work uses a non-smooth approach. In this case the non-smooth behavior of a system is modeled without the need to smooth the increase of contact forces for numerical reasons. In the case of contact, it can be assured that there is no penetration between contacting bodies. Overall, there are works that consider frictional behavior with an estimated COF, but to the best of the author's knowledge, there exists no work that implements a COF which depends on influencing parameters, such as ambient temperature or contact pressure, in the field of soft robotics.

1.2 Contributions

The main contribution of this paper is to provide a friction map containing COFs for different influencing parameter with the aim of encouraging researchers to implement frictional behavior in their SRs models. We present frictional measurements and highlight the importance of friction modeling.

Following the example of the *Soft Robotics Materials Database* [8], which is a database for unified material constitutive models, and to carry forward the idea of open sourcing knowledge we provide an open source database of COFs, making them accessible to the soft robotics community.[1] The COF is sensitive to different factors such as the ambient temperature, the sliding speed between contact partners, the contact pressure as well as the contact partners' materials, and surfaces. Therefore, we present a friction map that lists the COF of different contact partners depending on contact pressure and ambient temperature. The overall aim is to publish a growing friction map that researchers can contribute to in order to provide reasonable COFs for various scenarios. We demonstrate the effectiveness of implementing frictional contact behavior in a finite element analysis (FEA). As a starting point, measurements for the silicone rubbers Ecoflex 00-50 and Dragonskin 30 are presented. According to the manufacturer *SmoothOn*, Ecoflex 00-50 and Dragonskin 30 have a shore hardness of 50 Shore 00 and 30 Shore A respectively [30, 31].

2 Contact modeling

The COF can depend on the ambient temperature, the sliding speed between contact partners, the contact pressure as well as the contact partners' materials, and surfaces. Therefore, a friction map that lists the COFs between different contact partners depending on contact pressure and ambient temperature is required. The influence of the contact pressure is particularly important for gripping tasks since these tasks require friction. In this case the contact pressure or normal force needs to be controlled in order to lift objects. Therefore this work will focus on the influence of the contact pressure. The influence of the sliding speed is not yet considered in this work. The friction map is then implemented in a finite element simulation to demonstrate the necessity of implementing frictional behavior, using a soft pneumatic actuator (SPA) used for a gripping task as an example.

The frictional behavior of elastomers is very complex including effects such as hysteresis and adhesion and is strongly dependent on factors such as the surface condition and roughness [32, 33]. For dry contact, a rather simple contact model can be used to describe the frictional behavior between solid bodies

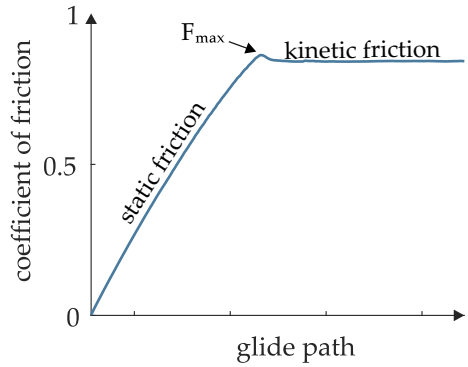

Fig. 3 Example friction measurement divided into static and kinetic friction

[34]: the coulomb friction model. It states that the frictional force F_R is proportional to the normal Force F_N times a coefficient - the coefficient of friction (μ) which leads to:

$$\mu = \frac{F_R}{F_N}. \tag{1}$$

Frictional behavior can be subdivided into two different cases [34]:

static friction:

$$F_{\mathrm{R,stat}} \leq \mu_{\mathrm{S}} F_{\mathrm{N}} \tag{2}$$

and kinetic friction:

$$F_{\mathrm{R,kin}} = \mu_{\mathrm{K}} F_{\mathrm{N}}. \tag{3}$$

The idea of using a coefficient to describe frictional behavior can be enhanced to use a COF that depends on multiple environmental influences such as ambient temperature or sliding distance [35, 36]. In Fig. 3, a qualitative example measurement of the COF over the sliding distance is shown. The COF rises steadily over measurement time and the related glide path until a maximum is reached. This point marks the maximum frictional forces that can be transmitted under the given condition. Up to this point, we assume gliding in the contact zone. In this case, only static friction occurs which is expressed by the static coefficient of friction μ_{S}. Thereafter, the COF settles at a constant value that can be lower or equal to the static COF as described for example in [37, 38]. In this case, the contact partners move relative to one another and the frictional behavior is described by the

[1] https://github.com/RebeccaBerthold/FrictionMap.

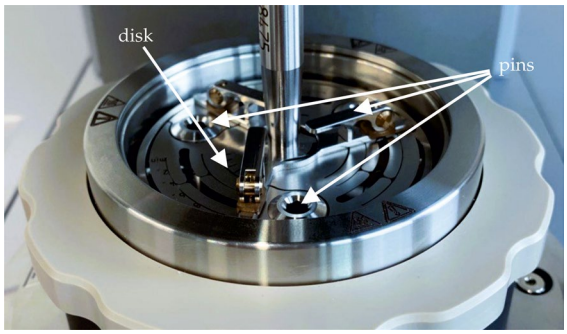

Fig. 4 MCR 302e rheometer showing pin-on-disc measurement setup without temperature-controlled chamber

kinetic coefficient of friction μ_K. The static frictional force $F_{R,stat}$ increases until the maximal force F_{max} is reached which corresponds to the maximal transmittable force. At this point, relative motion can be detected and the contact partners begin to slide relative to each other. In the following measurements, the average COF refers to the average kinetic COF μ_K.

The COF depends on the two specific contact partners and can furthermore depend on:

- contact pressure p
- ambient temperature T
- sliding speed v

To address these dependencies, a friction map is created which provides a COF for different contact partners depending on the contact pressure and ambient temperature.

3 Friction measurement

The following section describes the conducted measurements and provides details on the measurement setup.

3.1 Experimental setup

All measurements were conducted with a pin-on-disc measurement setup on a MCR 302e rheometer (Anton Paar, Austria) with the T-PID/44 measurement cell (Anton Paar, Austria) as shown in Fig. 4. The frictional behavior of two different contact partners is determined for a translational motion on a circular path at a given ambient temperature. All measurements are conducted in a temperature-controlled chamber to ensure a constant ambient temperature, where the ambient temperature refers to the temperature that is set for a specific measurement. Three sample pins (radius 3 mm, height 6 mm) of the same material are mounted in the measurement cell. A disk (radius 30 mm, height 2 mm) mounted in the rheometer serves as a counterpart to represent the contact partners for the pins. During the measurement, the contact pressure as well as the sliding speed can be adjusted. In preparation for the measurement, the samples are mounted and placed in the temperature controlled chamber at least 10 min before the measurement to ensure the whole sample adopts to the ambient temperature of the following experiment. Note that the time is increased according to the difference between room and ambient temperature.

In a first measurement step, the measuring cell is moved so that contact is established between the sample pins and the disk. The pins are moved until the resulting contact pressure reaches a preset target pressure. After that, the friction measurement starts during which the preset contact pressure from the previous step is maintained at a constant value. The measuring cell with the sample pins starts to rotate at a constant rotational speed of 0.005 rpm. The resulting sliding speed between the measurement cell and the disk is 0.007 mm/s. Preliminary measurements have shown that good and reproducible measurement results can be achieved at the selected rotational speed. The sampling rate of the measurement is 10 Hz.

The sample pins are made of the softer of the two contact partners' materials, which are the silicone rubbers Ecoflex 00-50 and Dragonskin 30, to prevent from measuring ploughing. In cases where a high COF occurs between the pin and disk, it must be ensured that the COF corresponds to the friction between the contact partners, and not between the pin and clamping. For this purpose, the material is glued on a 3D printed adapter. A commercially available silicone adhesive (Loctite 495) is used for this purpose. Care must be taken to ensure that the adhesive remains only in the adhesive zone and does not run into the contact surface, thus causing a change in the measurement. Measurements are conducted on clean samples. For the sample disks the following material samples were used:

- steel
- acrylic glass
- aluminium sheet and lathed aluminium disk
- Ecoflex 00-50
- Dragonskin 30
- cardboard
- wood

These materials are chosen to represent a broad range of different contact partners for SRs. In order to account for self-contact or contact between two SRs measurements are conducted where both samples, i.e. the pins and the disk, are made out of the silicones. The friction is very high in these cases which is a challenge for the measurement. In this case, special care must be taken to ensure that the sample pins remain mounted correctly through out the measurements. First, the measurements were performed at a reference temperature of 20°C. Note that an overview of all measurements can be seen in Fig. 5. All measurements show the transition from static to kinetic COF over the sliding distance, for different influencing parameter.

3.2 Influence of contact pressure on coefficient of friction

First, the influence of the contact pressure on the COF was investigated at an ambient temperature of 20°C. Therefore measurements of both pin materials with the above described contact partners were performed with different normal forces. The contact pressure can be calculated using the normal forces as follows:

$$p_{\text{Contact}} = \frac{F_{\text{N,Pin}}}{A_{\text{Pin}}}, \tag{4}$$

where $F_{\text{N,Pin}} = \frac{1}{3}F_{\text{N}}$ is the normal force for each pin and $A_{\text{Pin}} = \pi r^2 = 28.27\,\text{mm}^2$ is the contact area.

The contact pressure is set based on Eq. 4 via the normal force of the measurement cell. The resulting contact pressures are 11.79kPa, 35.37kPa, and 58.95 kPa. In Fig. 5a, a measurement for Ecoflex and acrylic glass is shown as an example. The measurement was conducted at an ambient temperature of 20°C. It can be seen, that increasing normal forces lead to decreasing COFs. Each measurement is repeated two times in order to ensure repeatability. The resulting COF can be seen in table 1.

Table 1 Dependency of the coefficient of friction on the contact pressure for Ecoflex and acrylic glass example at an ambient temperature of 20°C

contact pressure p in kPa	μ_{K}
11.79	0.87
35.37	0.51
58.95	0.32

3.3 Influence of the ambient temperature on the coefficient of friction

Next, the influence of the ambient temperature on the COF was investigated. The measurement was conducted at two different ambient temperatures of 10°C and 20°C with the same normal force. In Fig. 5b, a measurement for Dragonskin and Steel with a normal force $F_{\text{N}} = 3\text{N}$ at ambient temperatures of 10°C and 20°C is shown as an example. The average COF for the lower ambient temperature of 10°C is 0.41 and 0.45 at the higher ambient temperature of 20°C. This difference was for example also observed in the case where a normal force of $F_{\text{N}} = 5$ N was applied, as shown in Fig. 5c. In this measurement, the average COF at the lower ambient temperature of 10°C is 0.31 and 0.36 at the higher ambient temperature of 20°C.

3.4 Influence of the surface topology on the coefficient of friction

The surface topology can influence the frictional behavior. In order to showcase the dependency of the COF on the surface topology, two samples of the same material with different surfaces were used. For the first measurement, an aluminium disk cut out of a sheet is used. In Fig. 5e, measurements at the two different ambient temperatures are shown. For the second measurement the aluminium disk was lathed, showing the ring pattern from the manufacturing process. The surface roughness was not further investigated. The example is made to show the influence of the surface texture to create awareness that the surface topology itself can influence the frictional behavior. The measurement results can be seen in Fig. 5d. The results show that the kinetic COF with a mean value of 0.56 is slightly smaller for the lathed aluminium sample disk which is 0.57 at an ambient temperature

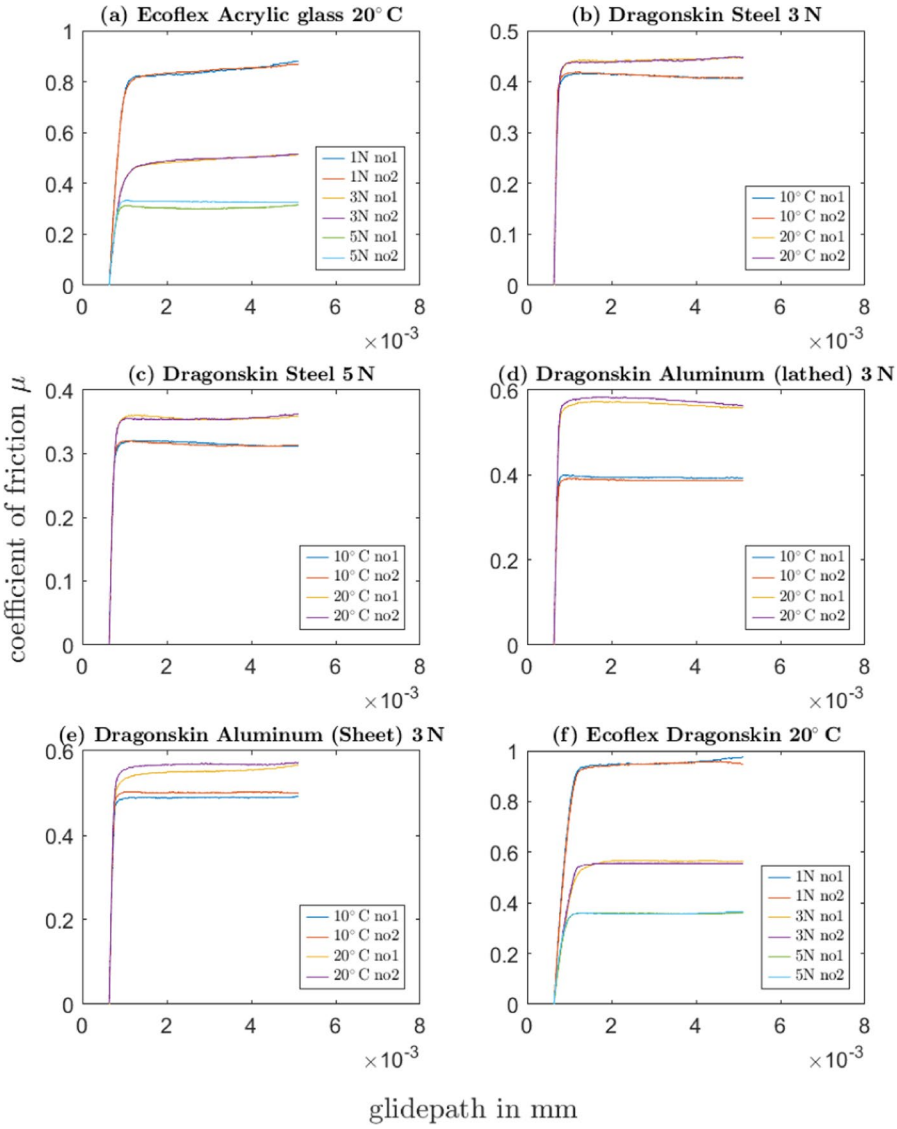

Fig. 5 Overview of the conducted measurements: **a** Ecoflex sample pin on an acrylic glass disk to demonstrate the influence of the contact pressure at a reference temperature of 20°C. **b** Dragonskin sample pin on a steel disk to demonstrate the influence of the ambient temperature with a normal force of 3 N. **c** Dragonskin sample pin on a steel disk to demonstrate the influence of the ambient temperature with a normal force of 5 N. **d** Dragonskin sample pin on a lathed disk subjected to a normal force of 3N and ambient temperatures of 10°C and 20°C. **e** Dragonskin sample pin on a smooth aluminum disk made from a sheet subjected to a normal force of 3 N and ambient temperatures of 10°C and 20°C. **f** Ecoflex sample pin on a Dragonskin disk to demonstrate the frictional behavior of self-contact with two silicone rubbers at an ambient temperature 20°C for various normal forces

of 20°C. At a lower ambient temperature of 10°C, the lathed aluminum's mean COF of 0.39 is significantly smaller than that of the smooth aluminum sheet, which is 0.5. This result demonstrates that surface topology has an influence on the frictional behavior and should be considered when using non-smooth surfaces.

3.5 Coefficient of friction for self-contact

To determine the COF for the self-contact case, the COF of Ecoflex and Dragonskin was measured. In Fig. 5f, the COF at an ambient temperature of 20°C and for different normal forces are shown. The measurements show that the COF of the silicone rubbers is significantly higher than the COF with any other contact partner. For a normal force of 1 N, the average COF is 0.96. The measurements show a comparably high COF for silicone contact, which should be taken into account for simulations involving self-contact or contact of multiple SRs.

3.6 Friction map

In the previous sections, individual COF measurements were presented and discussed. We

Table 2 Abstract of the friction map

material Pin	material Disk	contact pressure in kPA	ambient temp. in °C	COF μ_K
Dragonskin	acrylic glass	11.789	10	0.57
Dragonskin	acrylic glass	35.37	10	0.39
Dragonskin	acrylic glass	58.95	10	0.33
Ecoflex	wood	11.79	20	1.09
Ecoflex	wood	35.37	20	0.82
Ecoflex	wood	58.95	20	0.68
Dragonskin	cardboard	11.79	20	0.71
Dragonskin	cardboard	35.37	20	0.62
Dragonskin	cardboard	58.95	20	0.58
Dragonskin	Steel	11.79	20	0.63
Dragonskin	Steel	35.37	20	0.45
Dragonskin	Steel	58.95	20	0.36
Dragonskin	Steel	82.52	20	0.3
Dragonskin	Steel	106.1	20	0.26
Ecoflex	steel	11.79	10	0.91
Ecoflex	steel	35.37	10	0.49
Ecoflex	steel	58.95	10	0.36
Dragonskin	Dragonskin	35.37	10	0.48
Dragonskin	Dragonskin	82.52	20	0.28
Dragonskin	Ecoflex	11.79	20	1.08
Dragonskin	Ecoflex	58.95	20	0.89

summarize our measurement results in a friction map in Table 2. For readability, we limit the table to a subset of entries and refer the reader to the open access friction map for the full set of measurements. The friction map may be used to find the appropriate COF for a specific simulation. Furthermore, the friction map can be used to interpolate a COF if the needed COF was not listed, providing the basis for a more reliable contact simulation.

4 Contact simulation

In order to demonstrate the difference between frictional and non-frictional contact and moreover the influence of varying COFs, we conducted a series of measurements in finite element simulation (*ABAQUS* Dassault Systemes).

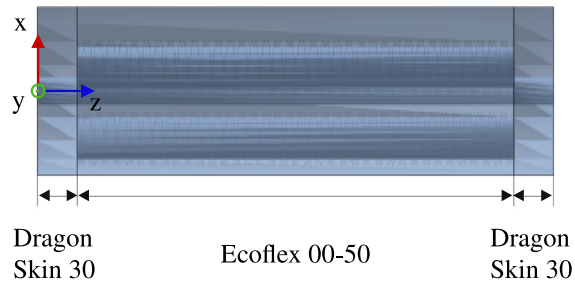

Fig. 6 Schematic figure of the soft pneumatic actuator with three fiber-reinforced chambers according to [39]

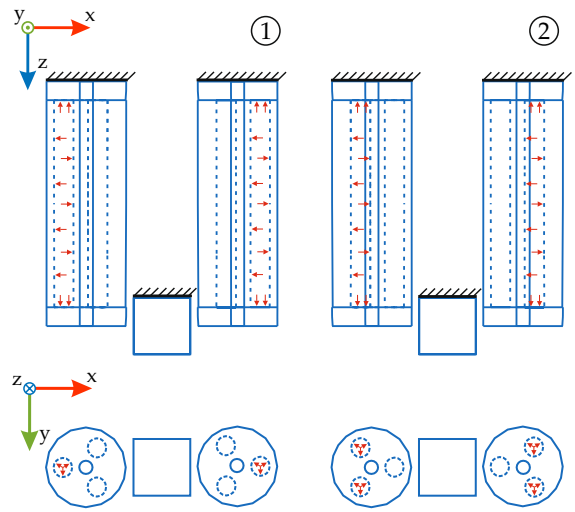

Fig. 7 Simulation setup for gripping a cube with different input pressures

4.1 Soft robot example

For this paper, we simulate the behavior of a soft pneumatic actuator, a common testbed for soft robotics research [39]. The SPA has three pneumatic chambers radially distributed around the actuator's longitudinal axis as shown in Fig. 6. Each chamber is fiber-reinforced to prevent the actuator from ballooning. In this example, the main body is made of a soft silicone rubber named Ecoflex 00-50. At either end, the body is supported with two stiff caps to prevent the cross section from significantly deforming. Both caps are made of Dragonskin 30. For the following simulation, a second actuator was added to the model to account for a common application and to form a gripper.

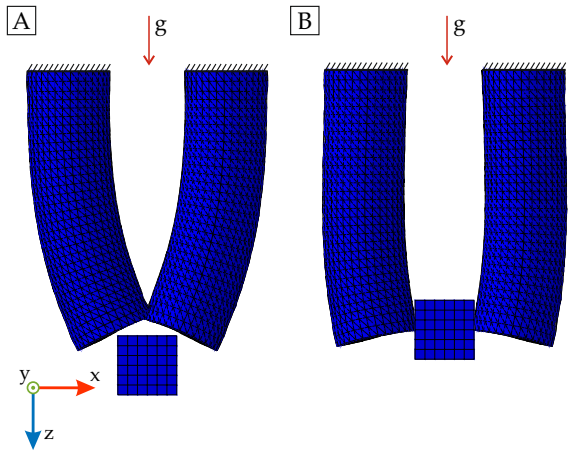

Fig. 8 Example results for a simulation with non-frictional contact **A** and frictional contact **B**

4.1.1 Finite element simulation

For the simulation, both silicones are modeled with a hyperelastic Ogden material model. The supporting fibers are modeled using beam elements and elastic material properties. More details on the model and specifically the material models can be found in [39]. A cube (mass= 54 g) is modeled as the object to pick up as shown in Fig. 7. Contact properties are defined between the SPAs and the cube. For normal and tangential contact, a penalty formulation was used. For the simulation, both pneumatic actuators are fixed at the top end while the bottom end can move freely. The first static simulation step consists of fixing the cube on its top surface and placing it 4 mm away from each actuator as shown in Fig. 7. In an additional static step, the actuators' chambers are inflated using a pressure load so that the SPA bends towards the cube and gravity is applied in the z-direction as shown in Fig. 8. In a last dynamic implicit step, the boundary condition of the cube is changed to allow for displacement in the z-direction induced by gravity. In this step the cube is only held by the gripping actuators. The simulation time for this step is 1 sec.

As demonstrated in Sect. 3.2, the contact pressure and the resulting normal force influence the COF. To demonstrate the impact of this effect, the described simulations are performed with different chamber pressures which result in varying contact pressure between the actuator and the cube. In *ABAQUS*, COFs can be defined depending on the slip-rate, contact pressure, and ambient temperature. The friction map for the Dragonskin-steel contact pair (given in table 2) is implemented in *ABAQUS* for the tangential interaction property. A finite sliding formulation with a surface-to-surface contact discretization was chosen. The simulation is performed at an ambient temperature of 20°C so the COF is implemented for a constant temperature. Values for the COF between the measured discrete values are linearly interpolated [18]. In *ABAQUS*, a critical shear stress $\tau_{crit} = \mu p$, which is defined by the COF μ and the contact pressure p, represents the maximal transmittable tangential force. It marks the transition before the state of sticking changes to gliding. If contact occurs, a constraint is applied to each node that is detected to be in contact.

Scenario: single chamber actuation

(a) frictional and non-frictional contact, 80 kPa

In the first step of the analysis, the simulation is run with frictional and non-friction contact with an input pressure of 80 kPa in one chamber as shown in Fig. 7 on the left side (1). It is shown that the cube can only be held due to friction. In the case of non-frictional contact, the cube drops as expected (Fig. 8A). For frictional contact the cube is held by the SPAs as shown in Fig. 8B.

In the following simulation, input pressures of 50 kPa, 80 kPa, and 100 kPa are used to vary the contact pressure. The contact pressure as well as the displacement of the cube in the z-direction are evaluated. As expected, the contact pressure increases with increasing chamber pressure.

(b) frictional contact, 50 kPa

For the lowest input pressure of 50 kPa, the cube drops because the COF is too low to reach a sufficient tangential contact force at this contact pressure. In contrast to non-frictional contact the cube drops more slowly after 0.15 sec compared to 0.08 sec.

(c) frictional contact, 80 kPa

For an input pressure of 80 kPa, the cube moved 2.8 mm in the z-direction. This displacement indicates that the friction is still not sufficient to hold the cube but slows down the fall.

(d) frictional contact, 100 kPa

For an input pressure of 100 kPa, a displacement of 1.5 mm is detected after a simulation time of 1 second. After 5 seconds, the displacement settles at a value of 1.7 mm when one chamber is actuated. In

this case, the displacement is caused by a change in the cube's equilibrium point due to its weight.

Scenario: multi chamber actuation

In the next simulation, the actuators were rotated by 180° and two chambers were each pressurized to 100 kPa for each actuator as shown in Fig. 7 on the right side (2). The actuation of two chambers leads to an additional increase in the contact pressure.

(a) frictional contact, 100 kPa

For an input pressure of 100 kPa, a displacement of 1.2 mm is detected. It is shown that the maximum transmissible tangential force increases with increasing contact pressure, resulting in a lower displacement in the z-direction.

5 Conclusions

In this paper, the frictional behavior of commonly employed material in soft robotics is assessed experimentally. The coefficient of friction is provided in a friction map for common material combinations. Moreover, the resulting COFs were implemented in a finite element simulation to demonstrate how the choice of a COF influences the performance of a SRs with respect to a specified task. The simulation experiments demonstrate the importance of friction for SRs which come in contact with their environment. In this paper, we presented the influence of actuation pressure with respect to the frictional behavior of the SPA. For future work the input pressure can be optimally adjusted with respect to the object's weight, which can inform optimal control and actuation parameters which in turn can reduce actuation effort as well as material wear on the SPA. The presented friction map enables researchers to implement a pressure and temperature dependant COF for various materials. The COF is a function of velocity and also strongly dependent on the surface properties. Establishing and conducting experimental protocols to include these dependencies into the friction map and adding more measurements are subject to future work. The open source nature will enable sharing of results among the soft robotics research community.

Acknowledgements Funded by the Deutsche Forschungsgemeinschaft (DFG, German Research Foundation) under grant no. 405032969 as part of the priority program 2100 Soft Material Robotic Systems.

Funding Open Access funding enabled and organized by Projekt DEAL.

Declarations

Conflict of interest The authors have no financial or proprietary interests in any material discussed in this article.

References

1. Kim Sangbae, Laschi Cecilia, Trimmer Barry (2013) Soft robotics: a bioinspired evolution in robotics. Trends Biotechnol 31(5):287–294. https://doi.org/10.1016/j.tibtech.2013.03.002
2. Jessica B-K, Caleb Rucker D, Howie C (2015) Continuum robots for medical applications: a survey. IEEE Transact Robot 31(6):1261–1280. https://doi.org/10.1109/tro.2015.2489500
3. Angrisani L, Grazioso S, Di Gironimo G, Panariello D, Tedesco A (2019) On the use of soft continuum robots for remote measurement tasks in constrained environments: a brief overview of applications. In: 2019 IEEE international symposium on measurements & networking (M &N), pp 1–5. IEEE. https://doi.org/10.1109/IWMN.2019.8805050
4. Boyraz Pinar, Runge Gundula, Raatz Annika (2018) An overview of novel actuators for soft robotics. Actuators 7(3):48. https://doi.org/10.3390/act7030048
5. Hawkes Elliot W, Carmel Majidi, Tolley Michael T (2021) Hard questions for soft robotics. Sci Robot 6(53):abg6049. https://doi.org/10.1126/scirobotics.abg6049
6. Holland Dónal P, Park EJ, Polygerinos P, Bennett GJ, Walsh CJ (2014) The soft robotics toolkit: shared resources for research and design. Soft Robot 1(3):224–230. https://doi.org/10.1089/soro.2014.0010
7. Eulalie C, Thor MB, Frederick L, Zhongkai Z, Maxime T, Mario Sanz Lopez, Bruno Carrez, Damien Marchal, Olivier Goury, Jeremie Dequidt, Christian Duriez (2017) Software toolkit for modeling, simulation and control of soft robots. Adv Robot 31:1208–1224. https://doi.org/10.1080/01691864.2017.1395362

8. Marechal L, Balland P, Lindenroth L, Petrou F, Kontovounisios C, Bello Fernando (2021) Towards a common framework and database of materials for soft robotics. Soft Robot 8(3):284–297. https://doi.org/10.1089/soro.2019.0115
9. Wang H, Totaro M, Beccai L (2018) Toward perceptive soft robots: progress and challenges. Adv Sci 5:1800541. https://doi.org/10.1002/advs.201800541
10. Laschi C, Cianchetti M, Mazzolai B, Margheri L, Follador M, Dario Paolo (2012) Soft robot arm inspired by the octopus. Adv Robot 26(7):709–727. https://doi.org/10.1163/156855312X626343
11. Morin Stephen A, Shepherd Robert F, Wai Kwok Sen, Stokes Adam A, Alex N, Whitesides George M (2012) Camouflage and display for soft machines. Science 337(6096):828–832. https://doi.org/10.1126/science.1222149
12. Ilievski F, Mazzeo AD, Shepherd RF, Chen X, Whitesides GM (2011) Soft robotics for chemists. Angew Chem 50:1890–1895. https://doi.org/10.1002/anie.201006464
13. Elango N, Faudzi AAM (2015) A review article: investigations on soft materials for soft robot manipulations. Int J Adv Manuf Technol 80(5–8):1027–1037. https://doi.org/10.1007/s00170-015-7085-3
14. Shepherd RF, Ilievski F, Choi W, Morin SA, Stokes AA, Mazzeo Aaron D, Chen Xin, Wang Michael, Whitesides George M (2011) Multigait soft robot. Proc Natl Acad Sci United States Am 108(51):20400–20403. https://doi.org/10.1073/pnas.1116564108
15. Hao Y, Wang T, Ren Z, Gong Z, Wang H, Yang Xingbang, Guan Shaoya, Wen Li (2017) Modeling and experiments of a soft robotic gripper in amphibious environments. Int J Adv Robot Syst 14(3):172988141770714. https://doi.org/10.1177/1729881417707148
16. Campisano F, Ozel S, Ramakrishnan A, Dwivedi A, Gkotsis N, Onal CD, Valdastri P (2017) Towards a soft robotic skin for autonomous tissue palpation. In: ICRA2017, pp 6150–6155. IEEE computer society. https://doi.org/10.1109/ICRA.2017.7989729
17. Yahya E, Augusto V, Constantina L, Tao G, Saaj CM, Tommaso Ranzani, Matteo Cianchetti, Arianna Menciassi (2014) Finite element analysis and design optimization of a pneumatically actuating silicone module for robotic surgery applications. Soft Robot 1(4):255–262. https://doi.org/10.1089/soro.2014.0016
18. Dassault Systemes. Simulia user assistance 2018 - specifying frictional behavior for mechanical contact property options. Technical Report, (2018)
19. Emanuele V, Emanuele G, Katia C, Marco FB, Luigi L, Vincenzo Positano, Simona Celi (2021) Modeling biomechanical interaction between soft tissue and soft robotic instruments: importance of constitutive anisotropic hyperelastic formulations. Int J Robot Res 40(1):224–235. https://doi.org/10.1177/0278364920927476
20. Sangpradit K, Liu H, Dasgupta P, Althoefer K, Seneviratne LD (2011) Finite-element modeling of soft tissue rolling indentation. IEEE Transact Biomed Eng 58(12):3319–3327. https://doi.org/10.1109/TBME.2011.2106783
21. Auricchio F, Conti M, Ferrara A, Morganti S, Reali A (2013) Patient-specific finite element analysis of carotid artery stenting: a focus on vessel modeling. Int J Numer Methods Biomed Eng 29(6):645–664. https://doi.org/10.1002/cnm.2511
22. Weicheng H, Xiaonan H, Carmel M, Khalid JM (2020) Dynamic simulation of articulated soft robots. Nat Commun 11(1):2233. https://doi.org/10.1038/s41467-020-15651-9
23. Vikas V, Cohen E, Grassi R, Sozer C, Trimmer B (2016) Design and locomotion control of a soft robot using friction manipulation and motor-tendon actuation. IEEE Transact Robot 32(4):949–959. https://doi.org/10.1109/TRO.2016.2588888
24. Gamus B, Salem L, Gat AD, Or Y (2020) Understanding inchworm crawling for soft-robotics. IEEE Robot Autom Lett 5(2):1397–1404. https://doi.org/10.1109/LRA.2020.2966407
25. Lamping F, Seis R, de Payrebrune KM (2021) On the motion of a snake-like soft robot. Proc Appl Math Mech 20(1):e202000037. https://doi.org/10.1002/pamm.202000037
26. Shadab ZS, Martina M, Cecilia L, Matteo C (2021) Actuation technologies for soft robot grippers and manipulators: a review. Curr Roboti Rep 2(1–15):09. https://doi.org/10.1007/s43154-021-00054-5
27. Weicheng H, Mingchao L, Jimmy HK (2023) Modeling of magnetic cilia carpet robots using discrete differential geometry formulation. Extrem Mech Lett 59:101967. https://doi.org/10.1016/j.eml.2023.101967
28. Calisti M, Picardi G, Laschi C (2017) Fundamentals of soft robot locomotion. J Royal Soc Interface 14(130):20170101. https://doi.org/10.1098/rsif.2017.0101
29. Kun W, Qiang Tian (2023) A nonsmooth method for spatial frictional contact dynamics of flexible multibody systems with large deformation. Int J Numer Methods Eng 124(3):752–779. https://doi.org/10.1002/nme.7141
30. Smooth-On, Inc. Technical data bulletin ecoflex 00-50, (2023a)
31. Smooth-On, Inc. Technical data bulletin dragonskin 30, (2023b)
32. Savkoor AR (1986) Mechanics of sliding friction of elastomers. Wear 113(1):37–60. https://doi.org/10.1016/0043-1648(86)90055-4
33. Popov VL, Voll L, Li Q, Chai YS, Popov M (2014) Generalized law of friction between elastomers and differently shaped rough bodies. Sci Rep 4(1):3750. https://doi.org/10.1038/srep03750
34. Popov Valentin L (2010) Contact mechanics and friction: physical principles and applications. Springer, Berlin. https://doi.org/10.1007/978-3-642-10803-7
35. Vahid M, Chuanfeng W, Michael Nosonovsky (2012) Stability of frictional sliding with the coefficient of friction depended on the temperature. J Tribol 134(4):041601. https://doi.org/10.1115/1.4006577
36. Suh Nam P, Sin H-C (1981) The genesis of friction. Wear 69(1):91–114. https://doi.org/10.1016/0043-1648(81)90315-X
37. Ernest R (1951) The nature of the static and kinetic coefficients of friction. J Appl Phys 22(11):1373–1379. https://doi.org/10.1063/1.1699869
38. Persson BNJ, Albohr O, Mancosu F, Peveri V, Samoilov VN, Sivebaek IM (2003) On the nature of the static

friction, kinetic friction and creep. Wear 254(9):835–851. https://doi.org/10.1016/S0043-1648(03)00234-5

39. Berthold R, Bartholdt MN, Wiese M, Kahms S, Spindeldreier S, Raatz A (2021) A preliminary study of soft material robotic modelling: Finite element method and cosserat rod model. In: 2021 9th international conference on control, mechatronics and automation (ICCMA), pp 7–13. https://doi.org/10.1109/ICCMA54375.2021.9646194